NASA Reference Publication 1277

1992

NASA Wallops Flight Facility Air-Sea Interaction Research Facility

Steven R. Long
Wallops Flight Facility
Wallops Island, Virginia

National Aeronautics and Space Administration

Office of Management

Scientific and Technical Information Program

TABLE OF CONTENTS

1. INTRODUCTION

This publication serves as an introduction to the Air-Sea Interaction Research Facility at NASA's Wallops Flight Facility, part of Goddard Space Flight Center, and located on Virginia's Eastern Shore near Chincoteague, VA. The purpose of this publication is to provide background information on the research facility itself, including capabilities, available instrumentation, the types of experiments already done, those ongoing, and future plans. But first, let's consider why this unique facility is there.

2. RATIONALE

Air-sea interaction processes are complicated phenomena. The difficulty lies in the fact that all the motions are inter-related in a way that is highly nonlinear. As an example, take the well-posed problem of wind wave generation that has been the goal for generations of oceanographers and fluid dynamists: the solution is still elusive. To solve this problem, one must know the nonlinear wave-wave interactions, the details of momentum and energy fluxes, and the dissipation mechanisms of the waves. Thus the well-posed problem encompasses a host of subsets of inter-related problems, each of which has its own impasse, and the sum of them makes the total problem intractable. It is clear to all investigators that in order to make progress, one would have to break up the problem into single dynamic components. It is perfectly possible that the sum of the components can be different from the whole. However, we can gain a certain understanding of the complicated processes involved, and this is our goal.

While much can be learned from field observations from ships, buoys, and aircraft, the many processes that participate in air-sea interaction also need to be studied under controlled conditions in the laboratory. While laboratory experiments can not simulate open ocean conditions, participant processes can be modeled and better understood.

The well-posed component problems, once defined, can be solved either theoretically or experimentally. The theoretical solutions invariably involve simplifying assumptions, and the experimental solutions typically have unexpected complications. This is especially true for field experiments, which are by definition the ultimate tests of the truth. But the uncontrollable environmental conditions almost always make the results short of being complete (not the desired conditions, conditions too severe for safety, conditions not steady enough for a complete test set, etc.). Limited by the prohibitive cost of a full field test, laboratory experiments offer simple and inexpensive alternatives with the understood limitations on the dynamic variability. It is fully appreciated that the laboratory conditions cannot simulate the natural environment in total. It is, however, also realized that if a problem is clearly defined and its dynamic processes identified, a laboratory experiment will be the most cost-effective way to produce a reasonable answer as a guide for full field verification. The laboratory experiments are the intermediate steps toward the full solution of the problem. It is with this understanding that the NASA Air-Sea Interaction Research Facility (NASIRF) was conceived and constructed.

3. HISTORY

The construction of the NASA Air-Sea Interaction Research Facility (NASIRF) was initiated in 1975 to provide basic scientific research and support for the GEOS-3 and SEASAT-1 satellite remote sensing projects. Primary objectives are to use the laboratory to test theoretical results and to collect empirical data for the development of remote sensing techniques, in support of microwave remote sensor technique development for air-sea interaction studies. With this goal in mind, the
most important surface phenomena needing research are the variations of the short gravity or the gravity-capillary waves under the actions of wind and ambient currents. These short waves are the most amenable ones to laboratory studies. Therefore, the interactions of wind, waves, and currents are central processes to be studied.

The main wind-wave-current research tank was designed by John van Overeem together with Norden E. Huang and Steven R. Long. The construction started at Wallops in early 1975 under the direction of Ken Calvert, assisted by Cris Lankford, Ed White, and others from the Wallops machine shop. It was finished by the beginning of 1977, when the first experiments were done. The initial instrumentation and data processing systems were designed around the Hewlett-Packard 9825 desktop calculators then available, and was developed and interfaced by Steven R. Long with the assistance of Bob Snyder. The first test result based on data from the new facility on the probability structure of the wind wave surface was published in 1980, using a capacitance-type wave probe of a new self-zeroing design developed and constructed at Wallops by Bob Snyder. The first hydraulic wave generator from Chant Engineering was designed and installed by Dave Moltedo. The second identical unit for waves in the opposite direction was installed by Granville Taylor. The next step in instrumentation expansion was built around the 4 channel HP spectrum analyzer, the 5451C, based on the early HP1000E mini-computers, and developed by Steven R. Long with the assistance of Larry F. Bliven. With the development of the mini-computer, we were able to expand to 16 data input channels, and a vastly more flexible software environment by moving to the HP1000F mini-computer system, developed by Larry F. Bliven with the assistance of Steven R. Long. The final step to our current capability came full circle back to the desktop with the rise of the personal computer and its associated hardware and software. Using multiple PC's, the present automated capability for A/D data acquisition, control, timing, archiving, computing, and graphical output was developed by Steven R. Long.

A second square tank was constructed in 1989 by Empire Fiberglass Co., based on a design by Norden E. Huang, for directional wave-current interaction studies. It was installed by the Wallops machine shop crew led by Bill Herz, and fully plumbed by Brett Mariner and Eddie Procaccio. Limited by the facility funds, the tank has not yet been fully instrumented, but is being added to and gradually developed in annual increments.

4. THE PHYSICAL DESCRIPTION OF NASIRF

The main wind-wave-current interaction tank is shown in figure 1. The main test section is 60 ft (18.29 m) in length, 4 ft (1.22 m) in height, and 3 ft (0.91 m) in width. Its operational water depth is 2.5 ft (0.76m) with 1.5 ft (0.45 m) remaining for air flow.

The wind is generated by a Trane suction fan located at one end of the tank and driven by a 25 HP motor. An electronic control board (U. S. Varidyne 2000 Inverter) has been installed in 1991 to control on/off, the speed, and the direction of the fan blades digitally through a personal computer (PC), so that any steady wind velocity or variation between 0 and 20 m/s at a reference height of 0.1 m above the mean water surface can be programmed.

Water current can be generated within the tank by a pump driven by a 15 HP motor. The maximum current of 6000 gal/min (378.1 l/sec) can be recirculated through a 16 in (0.41 m) diameter pipe connecting the two surge tanks at either end of the tank. The pump is controlled by an identical electronic control board as is used for the fan. Steady current or any variation up to 0.5 m/s can be generated in either direction in the test section by PC control. Spatial current gradients in the tank over selected parts of the test section can be generated by installing a false bottom.

Waves can be generated by a hydraulically driven paddle at either end of the tank. The hydraulic drive system was fabricated by Chant Engineering, Inc. This wave paddle can be fully programmed through a personal computer (PC) to generate waves of any frequency and amplitude compatible to the test section and generating machinery. Since the shallow water limitation of the tank is for waves of 1.5 m in length, the frequency is limited to the corresponding wave frequency of about 1.0 Hz. The amplitude is limited by the power rating of the hydraulic driving system, which in turn limits the high frequency for the paddle motion to 10 Hz with small amplitude, with amplitude increasing as frequency decreases, giving an amplitude of about 0.05 m at 2 Hz.

A smaller tank just being completed consists of a test section of 8 ft x 8 ft (2.44 m) with an operational water depth of 1 ft (0.3048 m). It is equipted for variable currents running diagonally within the test section between two large reservoirs, as shown in figure 2. This smaller tank will permit the study of wave-current interactions that occur at an angle.

unique advantages is the Mercury Computer MC-3200AT add-in card using M-Shell software by Applied Coherent Technology for complete, programmable image processing. Additionally, an Hitachi and Panasonic VCR can record an experiment continuously for later frame grabbing and processing. These items are discussed in more detail in a following section.

B. RCA ProWonder CamCorder: This is available to make an overall visual and voice record of any experiment in the facility or in the field.

8. Analog to Digital and Digital to Analog Conversion:

Data Translation and Keithley cards are used within the personal computers to digitize incoming data and to provide the outgoing control for the various equipment used by the facility. Each card has 16 analog to digital conversion channels, 2 digital to analog conversion channels (each with a maximum of +/- 10 v DC), and 2 16-bit digital I/O ports. The facility's maximum input data channel capacity is limited only by the number of A/D cards and computers available.

5.2 Recording Devices

1. Analog (FM) Data Recorders:

A. Honeywell 14 Ch.: Using 1 inch magnetic Tape, this recorder can take up to 14 channels of data, or 13 channels of data while using the 14th for a sync signal to guarantee the maximum accuracy in speed control on playback.

B. Hewlett-Packard 4 Ch.: Using 1/4 inch magnetic tape, this recorder can take up to 4 data channels.

C. TEAC 7 Ch.: Using instrumentation-grade cassette tapes, this recorder can take up to 7 channels of data, and operates off a dc voltage supply for in-lab use, or off a battery supply for field use.

2. Video Recorders:

A. Hitachi: A Hitachi model HS-423UR S-VHS 4 head VCR is available to record video images and/or sound in standard or S-mode.

B. Panasonic: A Panasonic model 7600 professional editing VCR is available to record or edit video images and/or sound in standard mode. Additionally, a BCD video controller is available to control all functions of this VCR through the imagine processing PC, allowing fully automated image processing to be developed in the Pascal language, or in real time from the PC keyboard using the BCD command set.

3. Digital Data Recording and Archiving: A Digi-Data model 2010 9-track digital magnetic tape recorder is used to archive raw data, programs, images, and results that have been previously

acquired by the personal computers (PC) as digitized data or processed results. It can also be used to exchange large amounts of data between the laboratory's personal computers, or using the Tape View software described in a following section, read or write data in any standard magnetic tape format, to allow data to be exchanged between the facility and other computers.

5.3 Data Processing

A variety of data processing is already available, and other specialized approaches can be easily developed within the following environments.

1. ASYST: A threaded subroutine language for the PC, allowing words to be defined in terms of ASYST library words, while these new words can then be used within further new words until the final program is a single word. With this concept, A/D and D/A can be easily controlled and timed, various statistics and analysis can be done, as well as graphical output or data output to other software packages.

2. Easyest: A non-programming approach shell around the ASYST environment, using a windowed display.

3. MatLab 386: A language environment making use of the complete capabilities of the 386 and 486 processors, in matrix notation, including a large capability in digital filtering and transformations, with complete graphical output or data output to other software packages.

4. DADiSP: A window-oriented, non-programming approach using a lab book concept where the data is input at the first window (or page), and the processing steps occur in subsequent windows. Results can be output as graphs, printouts, or output to other software packages.

5. Global Lab: A Data Translation product featuring complete control of Data Translation A/D and other I/O cards, as well as spectral analysis and other statistics.

6. ViewDAC: A multi-task managing environment specific to the 386 and 486 processor family that provides simultaneous control over multiple A/D, D/A, and digital I/O cards, as well as display of results or ongoing process development in a windowed display.

7. Lotus 123: Latest version of the popular spreadsheet product for analyzing experimental results. Includes graphical output capability.

8. SlideWrite Plus: Latest version incorporating mouse and windowed displays for graphing the results of the experiment in final, camera-ready format.

9. Golden Graphics: Latest version of Grapher (Complete 2D) and Surfer (Contours and Topographical Surfaces), for graphing the results of the experiment in final, camera-ready format.

10. Image Processing:

A. DT-Iris: An image processing environment furnishing a complete callable library for image enhancement, edge detection, filtering, false coloring, etc., and callable from C, Pascal, and Fortran.

B. Image Pro: An image processing environment using pull-down menus with mouse selection, and macro-script capability for doing repetetive operations, with edge detection, filtering, false coloring, etc.

C. M-Shell: A C-like programming environment for complete image processing using a Mercury Computer model MC-32-AT-IO-6 dedicated image processing card which uses the PC as a front end. The unique features of this package are its speed and ability to do 2D FFTs of the image.

11. Programming Languages: In addition to those already listed, the following are also available for use in the facility's PC's:

A. Microsoft C
B. Microsoft Pascal
C. Borland TurboPascal
D. GWBasic

12. Network Links: The facility PC's are linked via EtherNet to the Observational Science Branch Local Area Network to allow further data exchange and processing both locally and remotely.

5.4 Other Processing

In support of direct data processing, other processing is available as follows.

1. Word Processing: Two major packages are available to support the reporting of results in scientific journals.

A. WordPerfect: Latest version. All major functions of general word processing packages.

B. MASS-11: Latest version. All major functions of word processors with the added capability of easily including equations of every complexity within the text and viewed directly within the text on the processing screen.

2. Data Base: The latest version of Borland Paradox 386 is available for use.

3. Workstation: A Silicon Graphics IRIS Indigo workstation linked to the local network and gateway is available for more complicated image processing and wavelet analysis.

5.5 Utilities

Several utilities are available to support the operation of the facility personal computers.

1. Brief: Latest version of the popular full-featured programmer's editor.

2. Norton Utilities: Latest version of the popular disk support utilities.

3. XT Pro Gold: Latest version of the disk support utility, with new archiving features.

4. Communication Support: Latest versions of the popular communication packages:

   A. CrossTalk XVI

   B. ProComm Plus

   C. Kermit

   D. Network Links

   E. Carbon Copy Remote PC Control

6. SPECIAL TEST CAPABILITY

Because of the full control of conditions, timing, and repeatability that is possible with the present facility, transient phenomena can be studied by repeating the process until an adequate amount of data is obtained for an ensemble average. Additionally, the fully automated experiments can be conducted overnight, during the normal work day, over the weekends, or whatever schedule is necessary to acquire the data in a timely fashion. With several PC's available, data processing can procede as soon as the data is obtained, even though further data collection is progressing.

7. EXAMPLES OF RESULTS

A number of studies have been conducted in the facility since its construction. Some salient results will be summarized as follows:

The Probability Structure of the Wind Wave Surface

The elevation of a given point in the ocean is the resultant of many wave components. Dynamically, since the interactions among the different components are weak (see, for example,

Phillips, 1977), their motions are largely regarded as independent. Consequently, under the central-limit theorem, the probability distribution of the surface elevation has been assumed to be Gaussian. But nonlinearity (though small) is not zero, and its influence in the probability structure has been shown by Phillips (1961) and Longuet-Higgins (1963) to be proportional to the wave slope, which requires the surface elevation probability to be non-Gaussian. No conclusive data were available to support the theoretical result until our laboratory data became available in Huang and Long (1980). Not only was the influence of nonlinearity proved quantitatively, but the relationship found to be

$$\text{skewness} = 8\pi\,\S$$

was later confirmed by field data (McClain et al. 1982). This simple relationship provides the possibility for determining the mean wave length of the ocean waves from altimeter data, as demonstrated by Walsh (1979).

In addition to the elevation probability, the joint elevation-slope probability is of great importance for remote sensing applications, particularly for altimeter data reduction, and electromagnetic bias correction. In a later study by Huang et al. (1984), a closed form non-Gaussian joint elevation-slope density function was proposed and verified by laboratory data. Comparisons between theoretical and experimental results are presented in Figure 5. A special case of this joint density function is the joint specular point-elevation density, which is the basis for altimeter height determination. The result can be seen in Figure 6. With these studies, the performance of an altimeter can be thoroughly evaluated.

The Sea State Effects:
Air-Sea Momentum Flux
Scatterometer Algorithm

As the wind blows over the ocean, energy and momentum from the wind are transmitted to the ocean across the interface. Waves are inevitably generated, which represent the most energetic motions at the surface layer of the ocean. In fact, a large portion of the energy is first transferred to the waves, which in turn then transfers it further into the ocean through wave breaking (Huang 1986). Waves of different scales constitute the surface roughness structure which actually controls the energy and momentum fluxes (Geerneart and Plant, 1990). Up until very recently, the role of waves in the air-sea interaction has totally been neglected.

Back in the early 1980's, we conducted a series of experiments to investigate the role of waves in determining the fluxes across the air-sea interface. Such studies are important not only for the fluxes, but also crucial for the scatterometer algorithm. In our studies, we reached the following conclusions:

(1) The drag coefficient is a function of the sea state. The drag coefficient relates the wind speed to the wind stress, which is also the flux of momentum. It can be shown that the drag coefficient is a function of a roughness length scale.

The formula we developed is

$$h_s = [(m-1)!]^{\frac{1}{2}} \left[\frac{1}{X_o}\right]^{\frac{(m-1)}{2}} \left[1 - \exp(-X_0)\sum_{p=2}^{m} \frac{(X_0)^{p-2}}{(p-2)!}\right] \left[\zeta^2\right]^{\frac{1}{2}},$$

where Xo =(2κg)/(u.n_0), from Huang et al. (1986). Clearly, from this formula the drag coefficient will be a function of the sea state.

(2) The development of the surface roughness structure is not monotonic. The design of the satellite scatterometer is based on the backscattering of off-nadir radar pulses by the selective Bragg scattering mechanism. Earlier measurements of the ocean microwave backscattering coefficient suggested that it was related to the wind speed by a power law expression, such as

$$\sigma_0 = \alpha\ U^{\beta}\ ,$$

where α and β are empirically determined constants. Data from Seasat-1, however, suggested that there was systematic bias in using such a simple model for the basis of the algorithm. Our laboratory data show that the development of the ocean surface roughness is much more complicated. The relationship between the backscattering coefficient and the wind speed can be highly non-linear. It cannot be simplified to a simple power law. In fact, the relationship can be non-monotonic sometimes. Our ongoing study also suggests that the variation is a function of the pre-existing sea state. Based on this finding, we believe that the algorithm for the scatterometer needs to be re-defined. This statement represented only a minority view when we first published our result in 1984 (JGR 89). But now, however, it has become a generally accepted statement in the air-sea interaction community (Brown, 1990).

Wave-Current Interactions

Wave-current interaction remains as one of the least understood wave dynamic phenomena. The most interesting and crucial consequence of the wave-current interaction is the blocking phenomenon, the condition when the wave is stopped at the point where the local current is larger in magnitude than the group velocity, but opposite in direction to the wave propagation. According to the accepted theory, the wave motions are governed at all times by the kinematic and dynamic conservation laws. Under the steady state condition, the blocking point becomes a mathematical singularity, for when the sum of Cg + U becomes zero, the action of the waves will have to increase without bound in order to maintain their product constant. Consequently, the energy of the waves will increase drastically, and, at the same time, the length of the waves will decrease correspondingly to maintain the constancy of the frequency and the action flux. If events were indeed following this description, a logical sequence would be that the waves should break violently long before the waves reached this singular point. Indeed, blocking has been proposed

as a principle to construct artificial breakwaters (Taylor, 1955).

Based on a recent study, we have established that it is possible to have non-breaking blocking when waves are propagating against strong currents. Our results offer qualitative proof that the wave action is indeed reflected as predicted by the theory of Shyu and Phillips (1990); quantitative proof, however, is still wanting.

The consequence of the reflection caused by non-breaking blocking could have important applications in remote sensing data interpretations. The classic wave-current interaction theory stipulates that at blocking the wave number can only be compressed by a factor of four. In the new reflection theory, however, the wave number can change from the original value all the way into the capillary range, the compression ratio thus being almost open ended. Furthermore, in the classic theory, the wave number compression occurs only near the immediate neighborhood of the critical point; while in the new reflection theory, the wave number compression could occur over a large region spanning the initial blocking point and the secondary blocking point, and beyond. For example, a 1 m/s current can cause a 2.5m long wave to reflect and be trapped. According to the classic theory, though, the minimum wavelength at the blocking will only be 64 cm, which is still too long for most microwave radars to sense. But the new theory will allow waves to exist ranging from the original wavelength down to capillary waves over the current gradient region, and thus offers a much better chance for microwave radar detection. This is, in all probability, the real mechanism for the image formation for the Synthetic Aperture Radar (SAR) over many geographic locations as reported by Fu and Holt (1984).

Other than its effects on SAR, this surface roughness generating mechanism can also influence the performance of the scatterometer, which relies on the generated roughness satisfying the Bragg condition to infer ocean surface wind. Over the global ocean, the currents in the strong boundary current systems can certainly change the wave field as discussed earlier. This change can cause errors in the presently used scatterometer algorithms. To exclude the current in the wind measurement is a possible way to avoid the error, as is the present practice. But the major current system sometimes coincides with the explosive growth of the near costal storms. For that reason, monitoring the wind stress over the current system becomes an important task. In order to be able to do so over any current system, the understanding of the processes of wave-current interaction is indispensable. Therefore, the mechanism of wave-current interaction really deserves more study from a remote sensing point of view.

Spectral Properties

Based on laboratory study and published field data, we have proposed a unified two-parameter wave spectral model for a generalized sea state, known as the Wallops Spectrum. The inputs for the spectrum are the peak frequency and the rms wave elevation. With these two parameters, one can compute the significant slope, § , defined as

§ = (rms elevation)/(wave length at spectral peak).

Typical cases of model comparisons with field data are shown in figure 7. The figures show that the Wallops spectrum can correctly model the peak enhancement, even though it is not explicitly invoked in the spectral model. Based on the Wallops spectral model, we also found that the two most important undetermined coefficients (the Phillips constant and the peak enhancement function) in the popular JONSWAP spectrum can be parameterized by the significant slope (§). The Phillips constant is defined by the constancy condition given as

$$\overline{(\zeta^2)}^{\frac{1}{2}} = \int_n f(n)\, dn,$$

which is the definition of the power spectrum. This equation, however, gives us an equation of the Phillips constant from the Wallops spectral model. The result of comparisons with observed data from both laboratory and field is shown in figure 8. The goodness of fit is beyond doubt.

The comparisons of the peak enhancement function with the various parameterization schemes are shown in figures 9a, b, and c from Huang et al. (1990). The traditional parameterization using either non-dimensional fetch or the non-dimensional wind could not model the trend of the peak enhancement function at all. The significant slope as the parameter, on the other hand, can indeed reduce the scattered data into a coherent trend.

Benjamin-Feir: The Nonlinear Dynamics of the Wind-Wave Interactions

The weak resonant nonlinear wave-wave interaction is the cornerstone of the modern wave theory. One prima facie evidence of the effects of such interaction is the Benjamin-Feir instability, which predicts the modulational instability of a Stokes wave train. The existence of the Benjamin-Feir instability has been reported time and time again from laboratory data, but conclusive evidence from the field has never been found. In a study of the wind-wave interaction, we found that the surface wind can actually suppress the Benjamin-Feir instability and stabilize the wave train. Figure 10 shows the effect of wind on the development of the instability. If further analytic study confirms this observation, the lack of field evidence for the Benjamin-Feir instability can be finally resolved, for over the open ocean there are always winds of various magnitudes.

Wind-Wave Initialization

Wind wave initialization has been at the center stage of air-sea interaction studies for many years. But it remains an unsolved problem. Existing theories of wind wave generation of water waves do not properly address waves at this crucial stage. A brief summary of some of the most popular theories are given as follows to illustrate this point:

a. Miles Theory: The Miles theory is based on a shear instability mechanism. This mechanism requires the existence of a wavy surface to form the matched layer. Therefore, the theory will not be used to predict the initialization of the waves from a flat water surface. Furthermore, for

the Miles instability to work effectively, the matched layer thickness has to coincide with the wind profile at its maximum curvature. Consequently, the Miles theory is the most effective when the ratio of the wind speed to that of the dominant phase velocity is around 10. Both of these restrictions renders the Miles mechanism to be a wind wave interaction rather than a generation mechanism.

b. Phillips Theory: The Phillips theory is based on a resonant mechanism between the pressure pulsation in the wind with that of the underlying waves. The theory proposes an initial value problem of no waves on the water surface. Thus theoretically, it can indeed be applied to the initialization of the waves. But the resonant condition requires the matching of the phase velocity and the wind component in the direction of the wave propagation. A requirement like this essentially excludes the small scale waves in the centimeter range that are observed as the first roughness elements on the wind-blown water surface.

c. Kelvin-Helmholtz Theory: The Kelvin-Helmholtz instability is based on the inviscid shear current instability. It correctly predicts the wave length of the most unstable wave on the water surface. But the shear waves have a phase velocity too low to match the free wave propagation.

In our laboratory study, we have established that the initial stage of the waves are indeed in the capillary-gravity range as predicted by the Kelvin-Helmholtz theory. But the phase velocity is much higher than their predicted value. The growth rate of the wave energy is also too high to be accounted for by any of the existing theories.

In the initial stage, the waves successively go through several stages starting from a regular waves to chaotic, and then returning to regular. Such behavior strongly suggests highly nonlinear transitions of modes. This problem is still under active investigation.

In addition to joint research projects with Harvard University, Columbia University, the University of Delaware and the Johns Hopkins University where the facility supported graduate research in the various Ph.D programs, the following articles in refereed journals resulted.

1976

1. On the variation and growth of wave-slope spectra in the capillary-gravity range with increasing wind. S. R. Long and N. E. Huang, J.Fluid Mech., 77, 209-228.

2. Observations of wind-generated waves on variable current. S. R. Long and N. E. Huang, J. Phys. Oceanogr., 6, 962-968.

1980

1. An experimental study of the surface elevation probability distribution and statistics of wind-generated waves. N. E. Huang and S. R. Long, J. Fluid Mech., 101, 179-200.

1981

1. A unified two-parameter wave spectral model for a general sea state. N. E. Huang, S. R. Long, C. C. Tung, Y. Yuen, and L. F. Bliven, J. Fluid Mech., 112, 203-224.

2. On the importance of the significant slope in empirical wind-wave studies. N. E. Huang, S. R. Long, and L. F. Bliven, J. Phys. Oceanogr., 10, 569-573.

1983

1. A non-Gaussian statistical model for surface elevation of nonlinear random wave fields. N. E. Huang, S. R. Long, C. C. Tung, Y. Yuan, and L. F. Bliven, J. Geophys. Res., 88, 7597-7606.

2. A study on the spectral models for waves in finite water depth. N. E. Huang, P. A. Hwang, H. Wang, S. R. Long, and L. F. Bliven, J. Geophys. Res., 88, 9579-9587.

1984

1. A new type of overshoot phenomenon in wind wave development and its implication in remote sensing of the ocean. N. E. Huang, C. L. Parsons, S. R. Long, L. F. Bliven, and Q. Zheng, J. Geophys. Res., 89, 3679-3687.

2. The non-Gaussian joint probability density function of slope and elevation for a nonlinear gravity wave field. N. E. Huang, S. R. Long, L. F. Bliven, and C. C. Tung, J. Geophys. Res., 89, 1961-1972.

3. The harp probe: an in situ Bragg scattering sensor. E. Mollo-Christensen, N. E. Huang, L. F. Bliven, and S. R. Long, J. Atmos. Oceanic Tech., 1, 358-371.

1986

1. Experimental study of the influence of wind on Benjamin-Feir sideband instability. L. F. Bliven, N. E. Huang, and S. R. Long, J. Fluid Mech., 162, 237-260.

2. An experimental study of the statistical properties of wind-generated gravity waves. N. E. Huang, S. R. Long, and L. F. Bliven, Wave Dynamics and Radio Probing of the Ocean Surface, edited by O. M. Phillips and Klaus Hasselmann, Plenum Publishing Co., New York, Chapt.7, 129-144.

3. An estimate of the influence of breaking waves on the dynamics of the upper ocean. N. E. Huang, Wave Dynamics and Radio Probing of the Ocean Surface, edited by O. M. Phillips and Klaus Hasselmann, Plenum Publishing Co., New York, Chapt.20, 295-313.

4. An analytical model for oceanic whitecap coverage. N. E. Huang, L. F. Bliven, S. R. Long, and C. C. Tung, J. Phys. Oceanogr., 10, 1597-1604.

5. A study of the relationship among wind speed, sea state, and the drag coefficient for a developing wave field. N. E. Huang, L. F. Bliven, S. R. Long, and P. S. DeLeonibus, J. Geophys. Res., 91, 7733-7742.

1987

1. Spectrum of breaking waves in deep water. C. C. Tung and N. E. Huang, J. Enginr. Mech., 113, 293-302.

2. The effect of wave breaking on wave spectrum in water of finite depth. C. C. Tung and N. E. Huang, J. Geophys. Res., 92, 5125-5130.

3. The effect of wave breaking on the wave energy spectrum. C. C. Tung and N. E. Huang, J. Phys. Oceanogr., 17, 1156-1162.

1988

1. An estimate of wave breaking probability for deep water waves. Y. A. Papadimitrakis, N. E. Huang, L. F. Bliven, and S. R. Long, Sea Surface Sound, edited by B. R. Kerman, Kluwer Academic Publishers, New York, 71-83.

1989

1. Probability function of breaking-limited surface elevation. C. C. Tung, N. E. Huang, Y. Yuan, and S. R. Long, J. Geophys. Res., 94, 967-972.

2. Laboratory studies of wave-current interaction: kinematics of the strong interaction. R. J. Lai, S. R. Long, and N. E. Huang, J. Geophys. Res., 94, 16201-16214.

1990

1. Wave spectra. N. E. Huang, C. C. Tung, and S. R. Long, The Sea, Vol. 9, edited by B. LeMehaute and D. M. Hanes, John Wiley & Sons, New York, 197-237.

2. The probability structure of the ocean surface. N. E. Huang, C. C. Tung, and S. R. Long, The Sea, Vol. 9, edited by B. LeMehaute and D. M. Hanes, John Wiley & Sons, New York, 335-366.

8. REFERENCES

Bliven, L. F., N. E. Huang, and S. R. Long (1986). Experimental study of the influence of wind on Benjamin-Feir sideband instability. J. Fluid Mech., 162, 237-260.

Brown, R. A. (1990). Surface fluxes and remote sensing of air-sea interactions. Surface Waves and Fluxes, Kluwer Academic Publishers, Dortrecht, 7-28.

Fu, L. L., and B. Holt (1982). SEASAT Views Oceans and Sea Ice with Synthetic Aperture RADAR. JPL Publication No.81-120, 200pp.

Geerneart, G. L., and W. J. Plant, eds. (1990). Surface Waves and Fluxes, Kluwer Academic Publishers, Dortrecht.

Huang, N. E., and S. R. Long (1980). An experimental study of the surface elevation probability distribution and statistics of wind-generated waves. J. Fluid Mech., 101, 179-200.

Huang, N. E., S. R. Long, L. F. Bliven, and C. C. Tung (1984). The non-Gaussian joint probability density function of slope and elevation for a nonlinear gravity wave field. J. Geophys. Res., 89, 1961-1972.

Huang, N. E. (1986). An estimate of the influence of breaking waves on the dynamics of the upper ocean. Wave Dynamics and Radio Probing of the Ocean Surface, O. M. Phillips and Klaus Hasselmann, eds., Plenum Publishing, New York.

Huang, N. E., C.-C. Tung, and S. R. Long (1990). Wave Spectra. In The Sea, 9, Wiley-Interscience, New York, 197-237.

Longuet-Higgins, M. S. (1963). The generation of capillary waves by steep gravity waves., J. Fluid Mech., 16, 138-159.

McClain, C. R., D. T. Chen, and W. D. Hart (1982). On the use of laser profilometry for ocean wave studies. J. Geophys. Res., 87, 9509-9515.

Mollo-Christensen, E., N. E. Huang, L. F. Bliven, and S. R. Long (1984). The harp probe: an in situ Bragg scattering sensor. J. Atmos. Oceanic Tech., 1, 358-371.

Phillips, O. M. (1961). On the dynamics of unsteady gravity waves of finite amplitude. Part2. J. Fluid Mech., 11, 143-155.

Phillips, O. M. (1977). The Dynamics of the Upper Ocean. 2nd ed., Cambridge University Press, New York.

Shyu, J.-H., and O. M. Phillips (1990). The blockage of gravity and capillary waves by longer waves and currents. J. Fluid Mech., 217, 115-141.

Taylor, G. I. (1955). The action of a surface current used as a breakwater. Proc. Roy. Soc. A, 231,466-478.

Walsh, E. J. (1979). Extraction of ocean wave height and dominant wavelength from GEOS-3 altimeter data. J. Geophys. Res., 84, 4003-4010.

9. LIST OF FIGURES

Figure 1. The main research tank at the NASA Wallops Flight Facility.

Figure 2. The specialized wave-shear current interaction research tank at NASA Wallops Flight Facility.

Figure 3. The proto-type laser device for instantaneous slope of the wave surface.

Figure 4. The 5 tube Pitot array for instantaneous frictional velocity and wind profiles.

Figure 5. Comparison of theory and measurement: The joint elevation-slope probability density. Case a: significant slope = 0.0068 ; Case b: significant slope = 0.0203; Case c: significant slope = 0.0323. The density contours become increasingly nongaussian as the values of significant slope increase.

Figure 6. Comparison of theory and measurement: The elevation-spectral point (slope=0) joint probability density, for the same cases as in figure 5.

Figure 7. The comparison of the Wallops two-parameter spectral model with other models for the power spectral density. Wallops spectrum (— - - —), JONSWAP spectrum (— · — · —), Pierson-Moskowitz spectrum (.....), and the field data (_____). (a) Argus Island, no=0.133 Hz, T = 0.01145; (b) W.Atlantic, no = 0.093 Hz, T = 0.00815; (c) Hurricane Ava, no = 0.087 Hz, T = 0.0072; (d) Hurricane Camille, no = 0.068, T = 0.00625.

Figure 8. (a) The variation of the equilibrium range coefficient, b, with the significant slope, T. (b) The variation of the equilibrium range coefficient, b, with the non-dimensional fetch, gx/u*2. Data references given in Huang et al. (1981).

Figure 9. Comparison of peak enhancement function, g, of various parameterization schemes with the Wallops model: (a)g vs. the external variable, nondimensional fetch (b) g vs. the coupling variable, nondimensional frequency (c) g vs. the internal variable, the significant slope, T.

Figure 10. Wind suppression of the Benjamin-Feir instability. Data from Bliven et al. (1986).

10. ACKNOWLEDGEMENTS

Norden E. Huang and Steven R. Long wish to acknowledge all those who had a part in constructing and assembling the facility. The helpful and positive attitude of the Wallops employees in developing and supporting the needed work has been and continues to be our biggest asset.

11. INVITATION

Those interested in co-operative research and/or wishing to receive the facility's schedule of research as it is published periodically are invited to contact us at the address below:

Norden E. Huang
NASA GSFC
Code 971
Greenbelt, MD 20771
(301) 286-8879 Office
286-6662 Secretary
286-2717 FAX

Steven R. Long
NASA GSFC / WFF
Code 972
Wallops Island, VA 23337
(804) 824-1034 Office
824-2526 Secretary
824-1036 FAX
824-1471 NASIRF

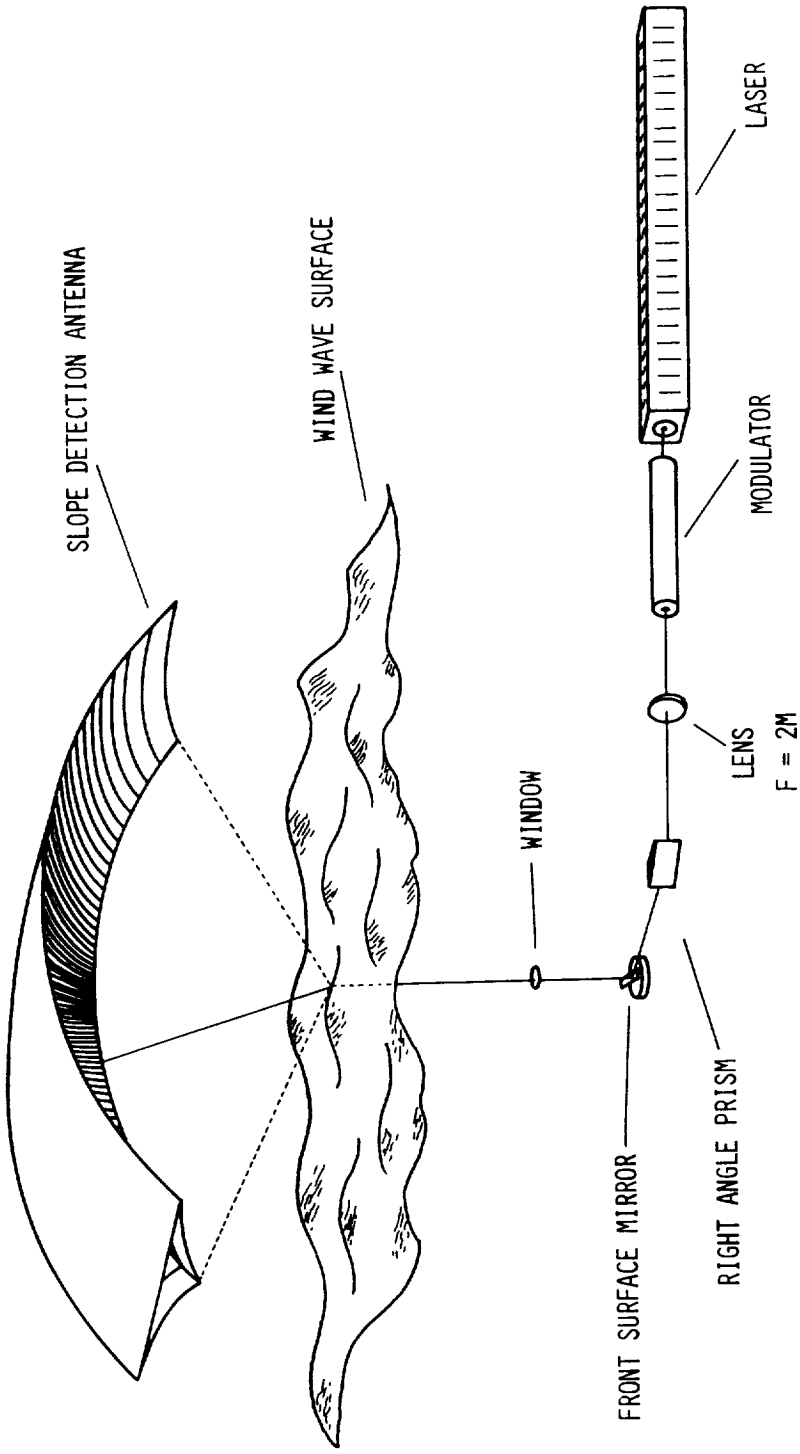

Figure 3. The prototype laser device for instantaneous slope of the wave surface.

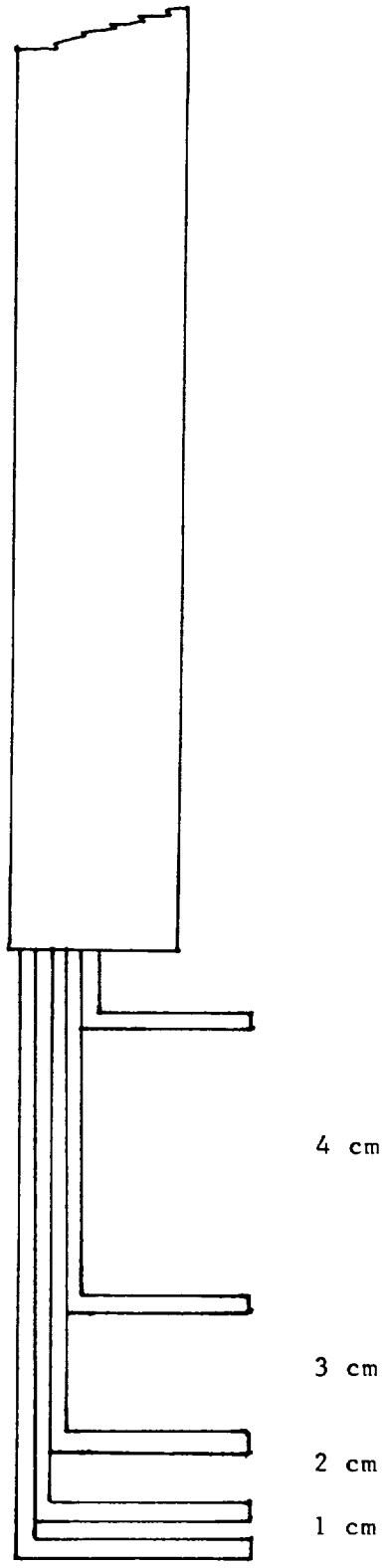

Figure 4. The 5-tube Pitot array for instantaneous frictional velocity and wind profiles.

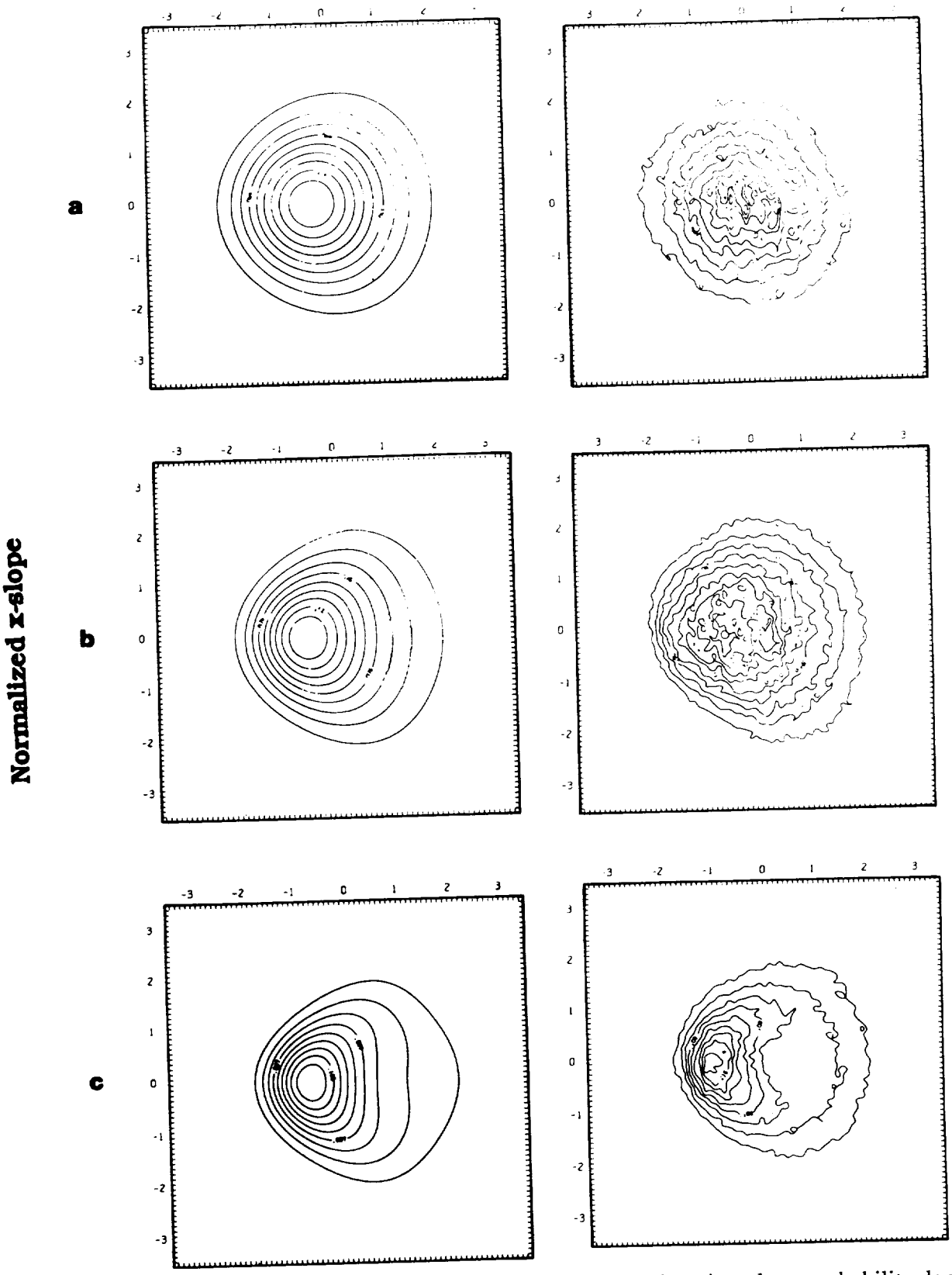

Figure 5. Comparison of theory and measurement: The joint elevation-slope probability density. Case a: significant slope = 0.0068; Case b: significant slope = 0.0203; Case c: significant slope = 0.0323. The density contours become increasingly nongaussian as the values of significant slope increase.

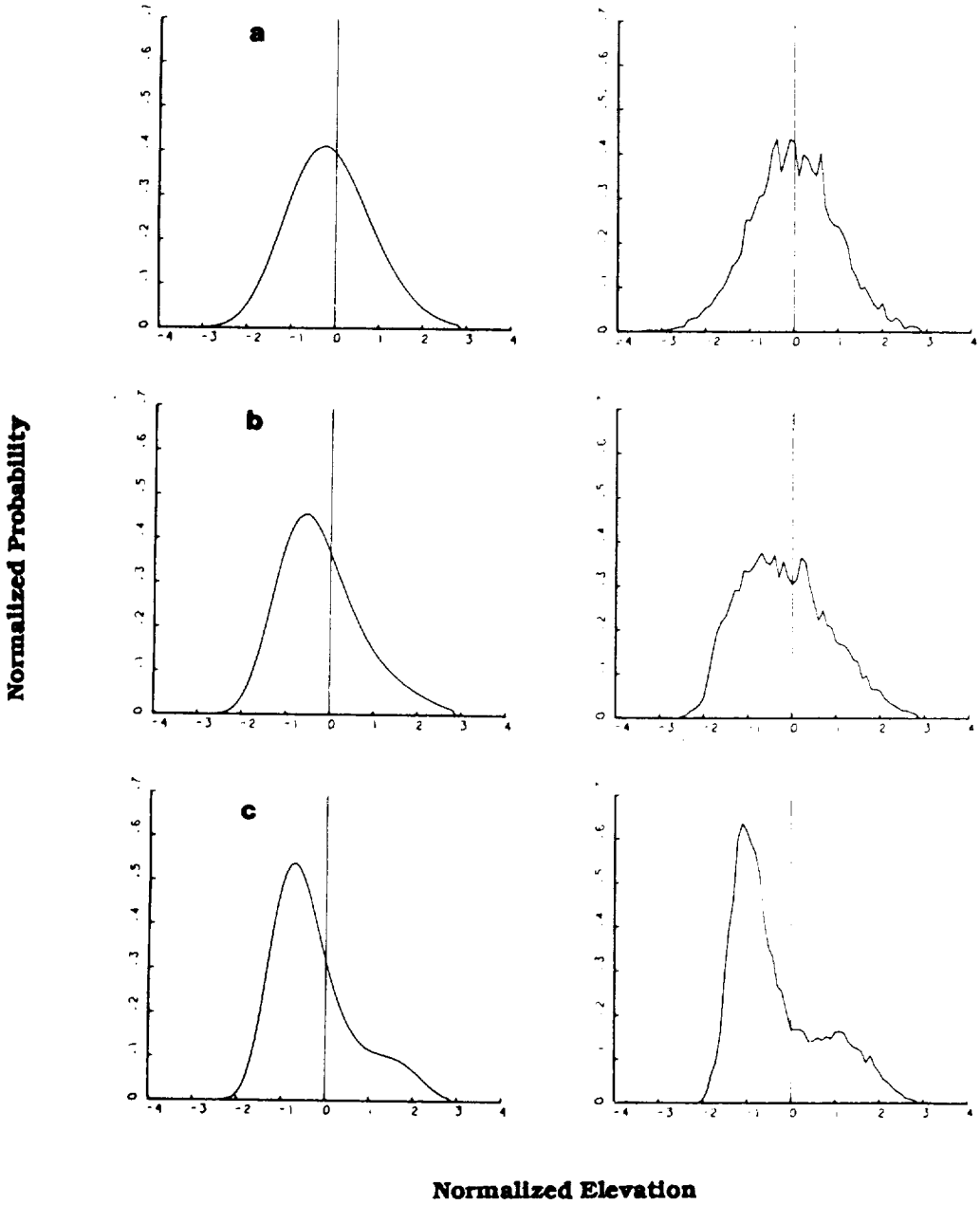

Figure 6. Comparison of theory and measurement: The elevation-spectral point (slope = 0) joint probability density, for the same cases as in Figure 5.

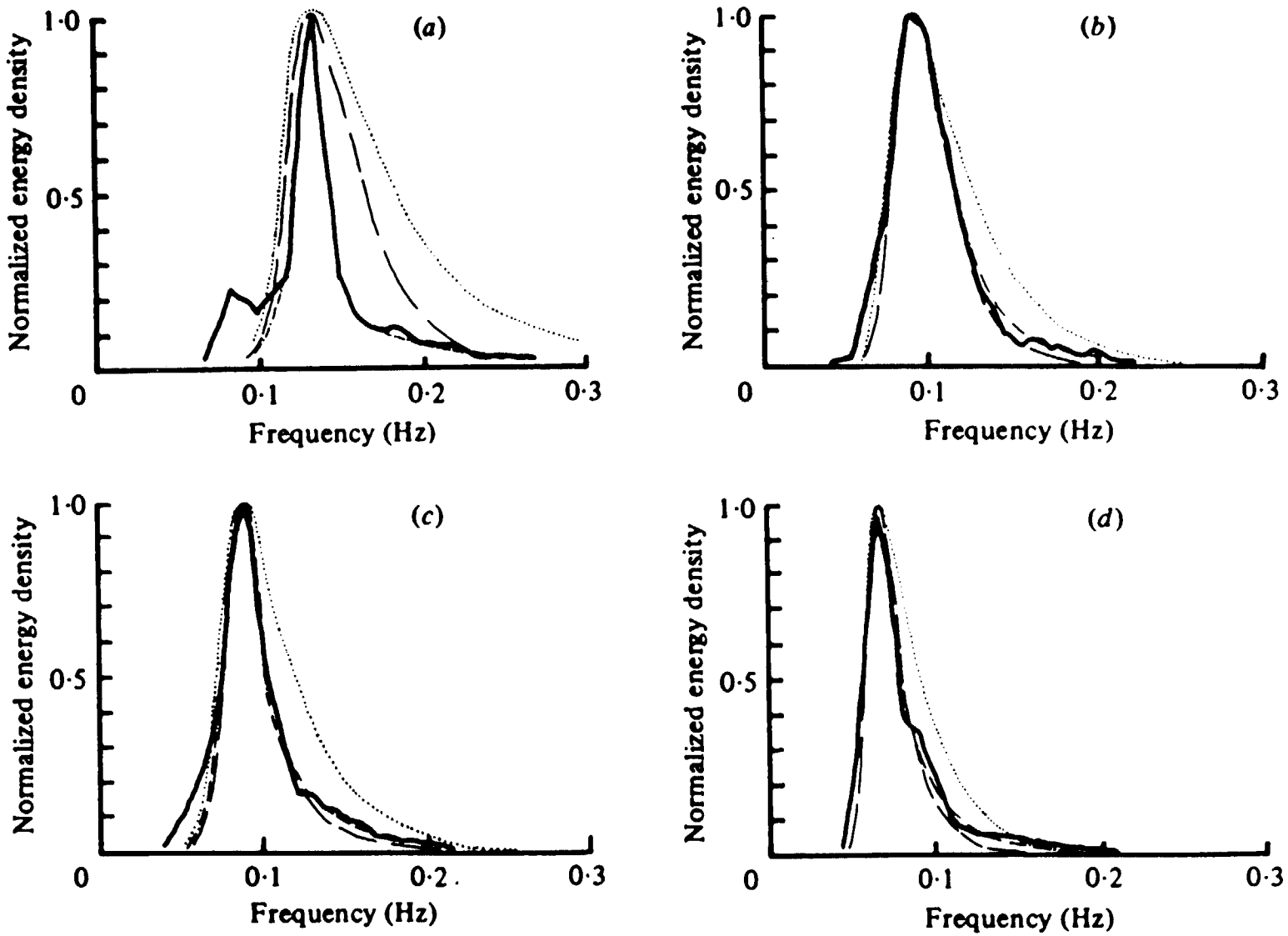

Figure 7. The comparison of the Wallops two-parameter spectral model with other models for the power spectral density. Wallops spectrum (——), JONSWAP spectrum (__ . __ . __) Pierson-Moskowitz spectrum (.....), and the field data (_____). (a) Argus Island, no = 0.133 Hz, T = 0.01145; (b) W. Atlantic, no = 0.093 Hz, T = 0.00815; (c) Hurricane Ava, no = 0.087 Hz, T = 0.0072; (d) Hurricane Camille, no = 0.068, T = 0.00625.

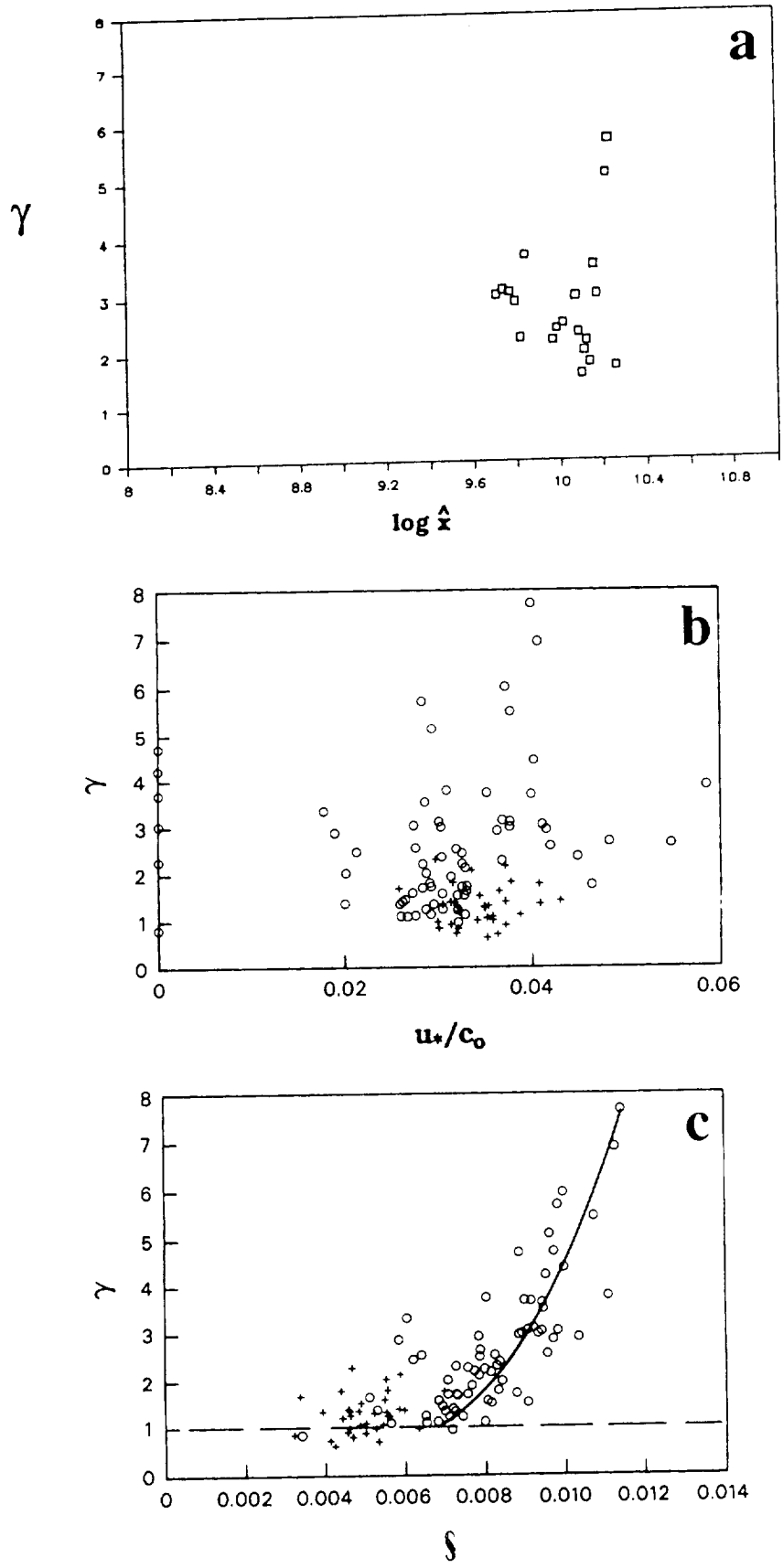

Figure 9. Comparison of peak enhancement function, g, of various parameterization schemes with the Wallops model: (a) g vs. the external variable, nondimensional fetch; (b) g vs. the coupling variable, nondimensional frequency; and (c) g vs. the internal variable, the significant slope T.

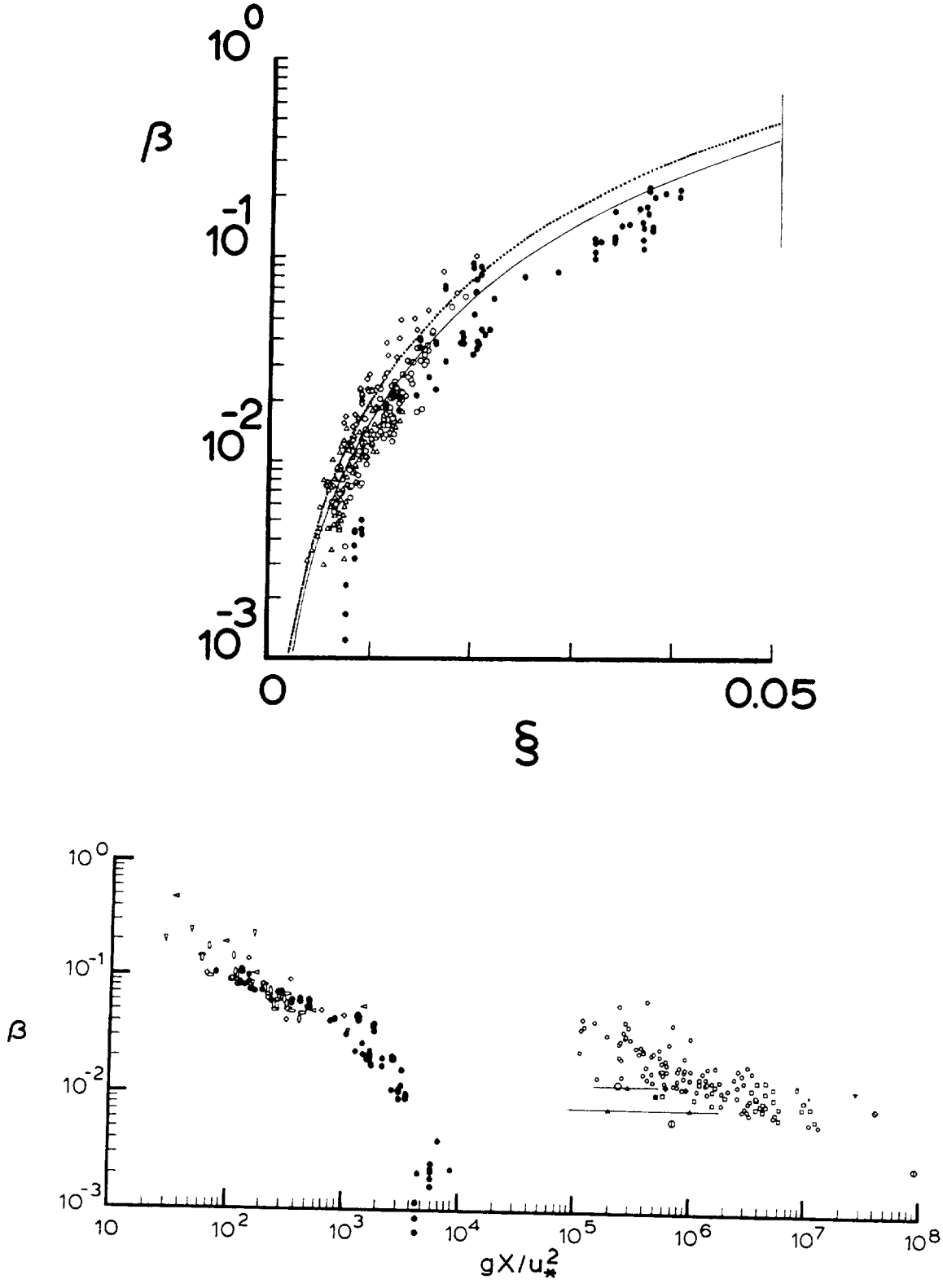

Figure 8. (a) The variation of the equilibrium range coefficient, b, with the significant slope, T. (b) The variation of the equilibrium range coefficient, b, with the nondimensional fetch gX/u_*^2. Data references given in Huang *et al.* (1981).

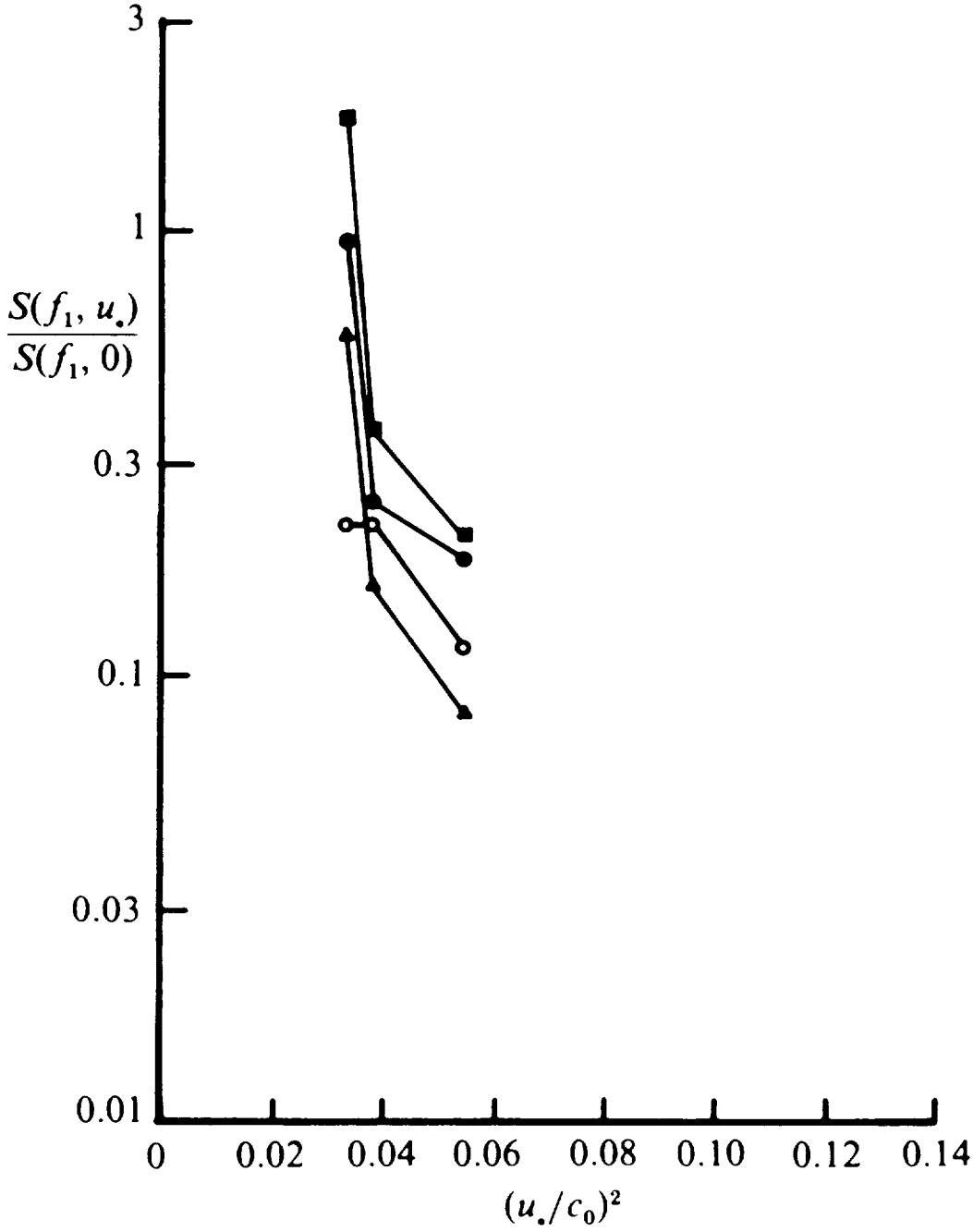

Figure 10. Wind suppression of the Benjamin-Feir instability. Data from Bliven *et al.* (1986).

REPORT DOCUMENTATION PAGE

Form Approved
OMB No. 0704-0188

1. AGENCY USE ONLY *(Leave blank)*	2. REPORT DATE	3. REPORT TYPE AND DATES COVERED
	June 1992	Reference Publication

4. TITLE AND SUBTITLE
NASA Wallops Flight Facility Air-Sea Interaction Research Facility

5. FUNDING NUMBERS
970

6. AUTHOR(S)
Steven R. Long

7. PERFORMING ORGANIZATION NAME(S) AND ADDRESS(ES)
NASA Wallops Flight Facility
Wallops Island, Virginia 23337

8. PERFORMING ORGANIZATION REPORT NUMBER
92B00059

9. SPONSORING/MONITORING AGENCY NAME(S) AND ADDRESS(ES)
National Aeronautics and Space Administration
Washington, D.C. 20546-0001

10. SPONSORING/MONITORING AGENCY REPORT NUMBER
NASA RP-1277

11. SUPPLEMENTARY NOTES
Steven R. Long, Code 972, NASA WFF, Wallops Island, Virginia 23337.

12a. DISTRIBUTION/AVAILABILITY STATEMENT
Unclassified - Unlimited
Subject Category 48

12b. DISTRIBUTION CODE

13. ABSTRACT *(Maximum 200 words)*

This publication serves as an introduction to the Air-Sea Interaction Research Facility at NASA/GSFC/Wallops Flight Facility. The purpose of this publication is to provide background information on the research facility itself, including capabilities, available instrumentation, the types of experiments already done, ongoing experiments, and future plans.

14. SUBJECT TERMS
Air-Sea Interactions, Wave Statistics, Ocean Surface Microscale

15. NUMBER OF PAGES
36

16. PRICE CODE
A03

17. SECURITY CLASSIFICATION OF REPORT	18. SECURITY CLASSIFICATION OF THIS PAGE	19. SECURITY CLASSIFICATION OF ABSTRACT	20. LIMITATION OF ABSTRACT
Unclassified	Unclassified	Unclassified	

NSN 7540-01-280-5500

Standard Form 298 (Rev. 2-89)
Prescribed by ANSI Std. 239-18, 298-102

NASA-Langley, 1992